Communication

An Optically Transparent Near-Zero-Index Grating Metamaterial for Enhanced On-Glass Millimeter-Wave Radiation

Ziheng Zhou, Yongjian Zhang, Zhicheng Kuang, Yue Li, and Zhizhang David Chen

***Abstract*— An optically transparent antenna (OTA) based on a grating metamaterial is proposed for launching high-gain millimeter-wave radiation on glasses. This design incorporates a glass-based dielectric image line with a grating made of a transparent conductive film (TCF), which provides an effective near-zero-index response through precise manipulation of spatial harmonic dispersion. To effectively overcome the intrinsic loss issue of TCF and control the power leakage, the field confinement in the grating metamaterial is engineered for optimizing the purely leakage-induced and total modal attenuations at the zero phase-progress state. The prototyped grating metamaterial antenna features an average optical transmittance of 76% over the visible spectrum. The antenna is validated to generate a near-broadside directive beam, achieving a realized gain exceeding 23 dBi and a total efficiency higher than 60% from 21.1 to 22.3 GHz. Through leaky mode confinement control and complex dispersion relationship engineering, this work offers a promising solution to realizing OTAs with a substantially improved gain and aperture efficiency.**

***Index Terms*— Antenna efficiency, grating, near-zero-index (NZI) metamaterial, optically transparent antenna (OTA), transparent conductive film (TCF).**

I. Introduction

The advances in the fifth/sixth-generation wireless communication and the Internet-of-Things technology have led to a growing demand for antennas with soft visual impact [1], [2], [3]. Against this background, optically transparent antennas (OTAs) [1], [2], [3], [4], [5], [6], [7], [8] are drawing intensive attention from both the academic and industrial communities. The OTAs are expected to implement the same wireless transceiving function as their conventional, opaque counterparts [9], [10], [11], [12] while simultaneously enabling efficient utilization of visible spectrum resources [13], [14], [15]. By integrating OTAs with diverse transparent platforms, including eyeglasses [15], [16], building windows [4], [5], [6], automobile windshields [17], [18], solar cell panels [19], [20], [21], and display screens [22], [23], [24], [25], much more physical space is opened up for establishing wireless connections. For example, Fig. 1 demonstrates two potential OTA applications: fixed wireless access in urban areas and forward obstacle detection for vehicles.

As a key material for constructing OTAs, the transparent conductive films (TCFs) have been intensively investigated, which include the indium-tin-oxide (ITO) films [4], [5], [6], meshed metal films (MMFs) [4], [5], [26], [27], [28], [29], [30], [31], conductive multilayer films [32], [33], [34], etc. For keeping high optical transmittance, the TCFs are manufactured with submicrometer- or nanometer-scale thicknesses, which are significantly smaller than their microwave-frequency skin depths and thus raise a severe ohmic loss issue. In comparison to the opaque copper sheets, the sheet resistances of MMFs are typically one order of magnitude higher, while those of ITO films can even be two orders of magnitude higher [4]. Due to high sheet resistances, the OTAs in current literature exhibit relatively lower gains than conventional opaque metal-based antennas. It was shown in [35] that the transparent patch antenna made of a conductive multilayer film offers a realized gain of −2 dBi. An optically transparent ITO monopole antenna investigated in [17] exhibits an optical transmittance of 70%, a radiation efficiency near 60%, and a realized gain of 2 dBi. An MMF patch antenna with an optical transmittance of 62% was proposed in [36], which offers a radiation efficiency of 43% and a realized gain of 2.6 dBi. An optically transparent cavity-resonator millimeter-wave (mmW) was proposed in [37], which exhibits an optical transmittance of 71%, a radiation efficiency of 45%, and a realized gain of 4.5 dBi. The development of OTAs with improved gain and radiation efficiency remains a grand challenge [38], [39], [40].

In this work, we propose an optically transparent leaky-wave metamaterial, in the form of a grating-loaded dielectric image line (DIL), for realizing a high-gain OTA. This structure exhibits an effective near-zero-index (NZI) leaky-wave state with low attenuation property, contributing to a more uniform aperture field distribution. The NZI materials and metamaterials with an infinitely stretched wavelength offer a unique platform for wave manipulation [41], [42]. Compared with the resonant-type NZI response [43], [44], the NZI effect derived from the spatially modulated leaky-wave structure exhibits higher material loss tolerance and is more advantageous for radiation applications. The innovation and contribution of the proposed design are outlined as follows. First, by manipulating the leaky mode's transverse confinement, strong field confinement on TCFs is avoided and the TCF's attenuating effect is effectively suppressed. Furthermore, the OTA's broadside gain and aperture efficiency are enhanced by engineering the complex propagation constant dispersion of the grating metamaterial at its NZI state.

Based on the proposed design philosophy, a 20-GHz OTA is prototyped using ITO films and quartz glass, characterized by an averaged optical transmittance of 76% over the visible spectrum from 400 to 760 nm. The prototyped OTA is experimentally validated to deliver a maximum realized gain of 23.6 dBi and a peak radiation efficiency of 67%. This competitive radiation performance is achieved under the usage of TCFs with much higher loss than opaque metal sheets. Hence, the proposed NZI grating metamaterial design would significantly boost the performance of mmW OTAs, opening up new prospects for ubiquitous wireless communication and sensing applications deployed on diverse optically transparent platforms.

II. Theoretical Modeling

The high sheet resistances of TCFs impose a challenge for achieving a uniform field distribution over a large-scale optically transparent aperture. To confront the intrinsic ohmic loss issue in the TCF-based

Received 13 December 2024; revised 20 January 2025; accepted 8 February 2025. Date of publication 28 February 2025; date of current version 4 June 2025. This work was supported in part by the Natural Science Foundation of China (NSFC) under Grant 62301162 and Grant U22B2016, in part by the National Key Research and Development Program of China under Grant 2021YFA0716601, in part by Fujian Provincial Natural Science Foundation of China under Grant 2023J01058, and in part by the Startup Funding of Fuzhou University under Grant XRC-23007. *(Corresponding author: Yue Li.)*

Ziheng Zhou and Zhicheng Kuang are with the College of Physics and Information Engineering, Fuzhou University, Fuzhou 350108, China.

Yongjian Zhang and Yue Li are with the Department of Electronic Engineering, Tsinghua University, Beijing 100084, China (e-mail: lyee@tsinghua.edu.cn).

Zhizhang David Chen is with the Department of Electrical and Computer Engineering, Dalhousie University, Halifax, NS B3H 4R2, Canada.

Digital Object Identifier 10.1109/TAP.2025.3543073

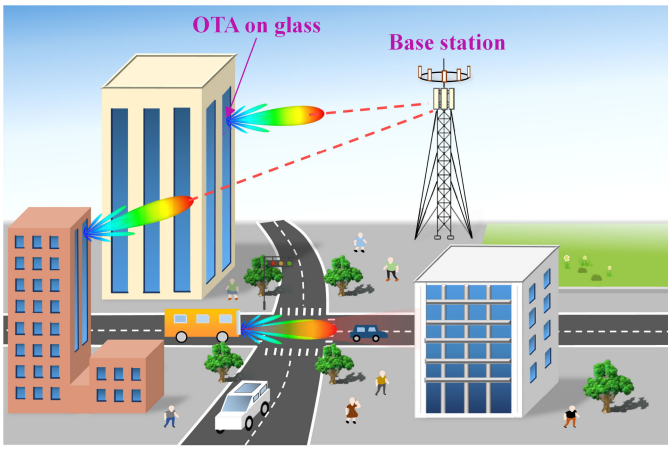

Fig. 1. Potential OTA applications in ubiquitous wireless communication and sensing, where OTAs are invisibly deployed on building windows and vehicular glasses.

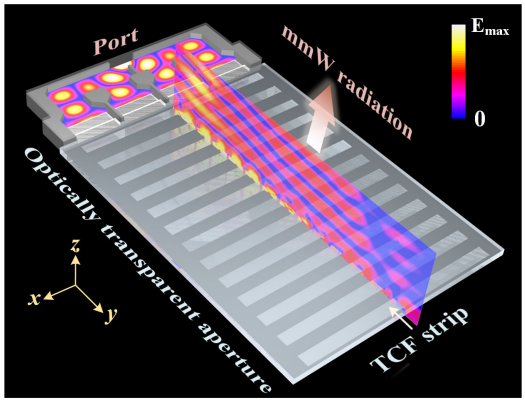

Fig. 2. Illustration of the grating metamaterial OTA along with the instantaneous electric field distribution.

OTA designs, this work presents an innovative solution that leverages complex dispersion engineering of leaky-wave metamaterials. This approach hinges on balancing the attenuation caused by power leakage and material absorption at the metamaterial's NZI radiative state, through which we suppress the total modal attenuation and excite high-gain broadside radiation.

Fig. 2 schematically illustrates the proposed OTA design based on a grating metamaterial, in which an optically transparent grating made of TCF couples the propagation mode in the glass substrate DIL to free-space radiation. The phase constant β_0 of the fundamental propagation mode in the unloaded DIL is governed by the dispersion equation [45]

$$\varepsilon_{\mathrm{r}}\sqrt{\beta_0^2-k_0^2}=\sqrt{\varepsilon_{\mathrm{r}}k_0^2-\beta_0^2}\tan\left(\sqrt{\varepsilon_{\mathrm{r}}k_0^2-\beta_0^2}h\right) \tag{1}$$

where ε_{r} and h denote, respectively, the dielectric constant and thickness of the glass substrate, and k_0 is the free-space wavenumber. A uniform field distribution in the DIL's width direction, i.e., the x-direction, has been assumed in (1). The periodic modulation of DIL through grating loading generates spatial harmonics with phase constants $\beta_n = \beta_0 + 2\pi n/p$, where n is an integer and p is the grating period. Here, we require the -1st-order spatial harmonic to have a near-zero phase constant, i.e., $\beta_{-1} \approx 0$. Under this condition, the grating metamaterial is characterized by an effective near-zero index that enables broadside radiation.

We then demonstrate the approach to regulate the attenuation constants caused by the material loss and power leakage at the grating metamaterial's effective NZI state. Examine the concrete grating-loaded DIL structure given in Fig. 3, where the dielectric

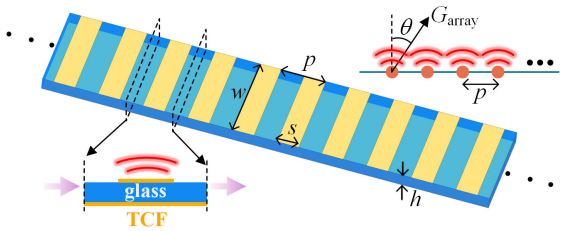

Fig. 3. Grating-loaded DIL structure and its equivalent array model.

constant of the quartz glass substrate is 3.65, DIL's width w is chosen as 21 mm, and the grating strip width is denoted by s. The grating structure and DIL ground are made of TCFs with resistances R_{s} being, respectively, 5 and 2 Ω/sq. The element of this periodically loaded DIL is shown in the left-bottom inset of Fig. 3. The complex propagation constant of $\beta - \mathrm{j}\alpha_{\mathrm{total}}$ the grating-loaded DIL is extracted via [45]

$$\cos\left[(\beta-\mathrm{j}\alpha_{\mathrm{total}})\,p\right]=(A_{11}+A_{22})/2 \tag{2}$$

where A_{11} and A_{22} are the entries of the metamaterial element's transfer matrix $\mathbf{A}$. We note that α_{total} accounts for the total modal attenuation due to leakage radiation, material losses, and stopband effect. Since the dielectric loss of quartz glass is negligible, the ohmic dissipation on TCF grating and ground is the cause of material-loss-related attenuation. The phase constant β in (2) is restricted in the light cone of the first Brillouin zone, i.e., the region of -1st-order spatial harmonic.

The grating-loaded DILs with thicknesses h of 1.5, 2.5, and 3.5 mm are investigated, where the corresponding grating strip widths s are 5.6, 4.8, and 2.0 mm, respectively. The grating period p for all three cases is fixed as 8.7 mm, i.e., 0.6λ at 20.8 GHz. As shown in Fig. 4(a), all the phase constant curves cross zero around 20.8 GHz, at which the grating metamaterial's effective refractive index $n_{\mathrm{eff}} = (\beta - \mathrm{j}\alpha_{\mathrm{total}})/k_0$ has a vanishing real part. The extracted total attenuation constants for the three cases are shown in Fig. 4(b). Although grating-loaded DILs in cases #1–#3 share the same NZI frequency, their phase dispersion and attenuation behaviors are distinctive. In Case #1, the unit cell consisting of a wide strip over a low-profile ($h = 1.5$ mm) grounded substrate acts as a thin cavity resonator, which exhibits a strong phase dispersion when $\beta \cdot p$ crosses zero. Its excessively thin substrate also leads to a high power leakage rate and intensity ohmic loss on TCFs, which manifests as a large α_{total}. For Case #3 with an excessively thick substrate ($h =$ 3.5 mm), although the strong phase dispersion is avoided, a severe open-stopband effect—indicated by a sharp rising of attenuation near the NZI frequency—is observed in Fig. 4(b). Between those extreme cases, the grating-loaded DIL in Case #2 with an optimized thickness $h = 2.5$ mm and strip width $s = 4.8$ mm features a small phase slope near NZI frequency and a moderate total attenuation constant primarily caused by radiation leakage. Since the DIL parameters have been specially engineered to accommodate the optically transparent leaky-wave antenna design with lossy TCFs, they are different from the typical values reported in [46].

To proceed, we examine the ratio of the radiation-induced attenuation constant (or power leakage rate) α_{rad} to the total attenuation constant α_{total}, which reflects the radiation efficiency of a leaky-wave structure [47]. For Cases #1 and #2 where the grating-loaded DIL operates in the passband, α_{rad} is equal to the attenuation constant with all the materials assigned lossless. For Case #3, open-stopband attenuation should also be excluded when calculating α_{rad}. According to Fig. 4(c), the grating-loaded DIL in Case #2 with optimized transverse structure parameters achieves the highest $\alpha_{\mathrm{rad}}/\alpha_{\mathrm{total}}$ around

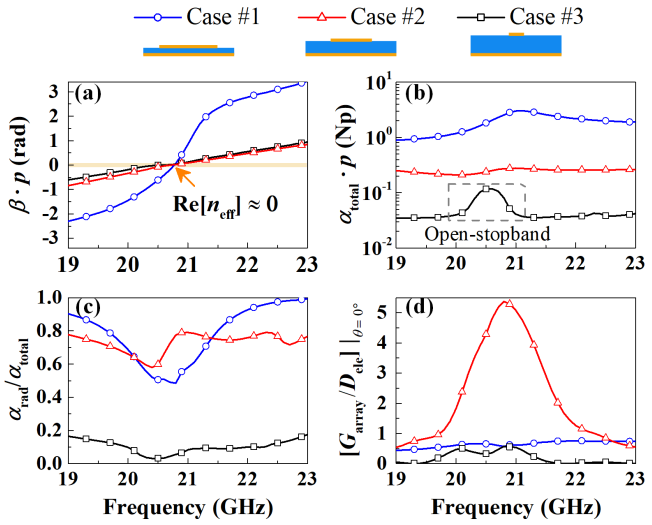

Fig. 4. (a) Phase constant dispersion. (b) Attenuation constant dispersion. (c) Ratio of $\alpha_{\rm rad}$ to $\alpha_{\rm total}$. (d) Broadside gain enhancement factor for the grating-loaded DILs in Cases #1–#3.

the NZI frequency, indicating an efficient broadside radiation performance. To quantitatively analyze the broadside radiation intensity of the proposed NZI grating metamaterial, we develop a simplified array model as shown in the right-top inset of Fig. 3, where the grating-loaded DIL structure is modeled as an array of radiators fed with a phase progress of $\beta \cdot p$ and attenuated amplitudes. The array gain function $G_{\rm array}$ dependent on the observation angle θ is formulated as

$$G_{\rm array}(\theta) = \left| \sum_{m=0}^{N-1} \sqrt{P_{{\rm rad},m}/P_{\rm in}}\, {\rm e}^{-{\rm j}[\beta - k_0 \sin(\theta)]mp} \right|^2 D_{\rm ele}(\theta) \quad (3)$$

where $D_{\rm ele}$ denotes the directivity pattern of the metamaterial array element. $P_{{\rm rad},m}/P_{\rm in}$ denotes the power radiated by the mth element normalized to the input power $P_{\rm in}$ of the array, and N is the total number of the elements. Over a length element dl along the leak-wave structure, the radiated power d$P_{\rm rad}$ is related to the transmission power decrease dP via

$$ {\rm d}P_{\rm rad} = 2\alpha_{\rm rad} \cdot P_{\rm in} \cdot e^{-2\alpha_{\rm total} l}\, {\rm d}l. \quad (4)$$

Integrating (4) on both sides over the length of mth unit cell leads to

$$\begin{aligned} \frac{P_{{\rm rad},m}}{P_{\rm in}} &= 2\alpha_{\rm rad} \int_{mp}^{(m+1)p} {\rm e}^{-2\alpha_{\rm total} l}\, {\rm d}l \\ &= \frac{\alpha_{\rm rad}}{\alpha_{\rm total}} \left(1 - {\rm e}^{-2\alpha_{\rm total} p}\right) {\rm e}^{-2\alpha_{\rm total} mp}. \end{aligned} \quad (5)$$

Then we define the following figure of merit (FOM) as the ratio of the array's broadside realized gain to the element's directivity, i.e.,

$$\begin{aligned} FOM &\equiv \frac{G_{\rm array}(\theta = 0^\circ)}{D_{\rm ele}(\theta = 0^\circ)} \\ &= \frac{\alpha_{\rm rad}}{\alpha_{\rm total}} \left(1 - {\rm e}^{-2\alpha_{\rm total} p}\right) \left| \frac{1 - {\rm e}^{-(\alpha_{\rm total} + {\rm j}\beta) Np}}{1 - {\rm e}^{-(\alpha_{\rm total} + {\rm j}\beta) p}} \right|^2. \end{aligned} \quad (6)$$

Maximizing this gain enhancement factor necessitates: 1) properly increasing the power leakage rate $\alpha_{\rm rad}$ and 2) keeping a low total modal attenuation constant $\alpha_{\rm total}$. Through the control of wave attenuation and leakage properties, enhanced radiation with an improved aperture efficiency is expected to be achieved. The calculated FOMs for the grating-loaded DILs in Cases #1–#3 are depicted in Fig. 4(d). The optimal design in Case #2 exhibits a notably higher gain enhancement FOM near the broadside-radiation frequency, which is attributed to its moderate total attenuation constant ($\alpha_{\rm total}$) and the maximized ratio of power leakage rate to total modal attenuation constant ($\alpha_{\rm rad}/\alpha_{\rm total}$).

TABLE I
OTA STRUCTURAL PARAMETERS (UNIT: mm)

l_0	w_0	a_0	a_1	a_2	a_3	d	b_0	b_1	Δ
118.0	76.0	10.7	10.0	5.6	17.0	19.0	9.0	3.0	6.0
s_1	s_2	s_3	s_4	s_5	p_1	p_2	p_3	p_4	p_5
3.7	4.0	3.7	4.0	4.4	9.9	9.2	9.3	9.4	9.1
$s_{6\text{-}13}$	$p_{6\text{-}12}$	h_1	h_2						
4.5	9.0	1.0	1.5						

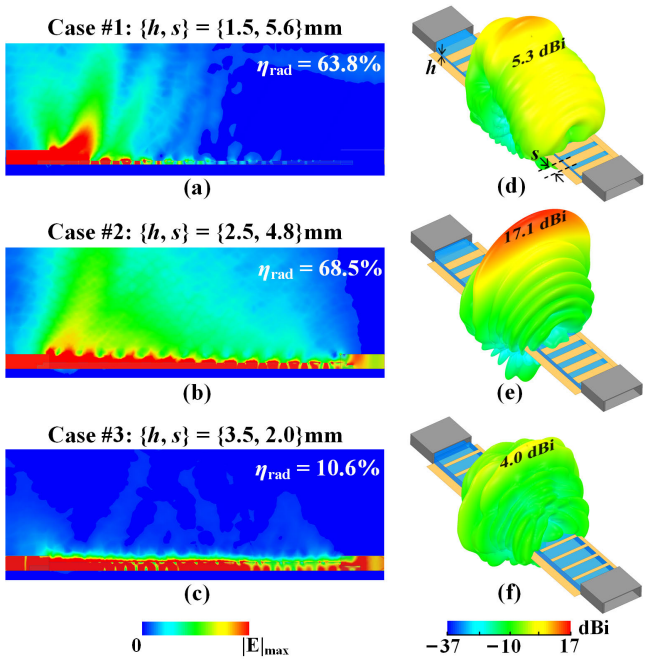

Fig. 5. (a)–(c) Simulated electric field magnitude distributions. (d)–(f) Realized gain patterns for the grating-loaded DILs in Cases #1–#3.

Fig. 5(a)–(c) displays the simulated electric field magnitude distributions at 20.8 GHz for the grating-loaded DILs in cases #1–#3, each having an aperture length of 8.3λ at 20.8 GHz. The grating-loaded DILs are excited using a rectangular waveguide operating on the fundamental TE_{10}mode. The corresponding 3-D realized gain patterns for the three cases are shown in Fig. 5(d)–(f). It is noted that the theoretically predicated metamaterial's refractive indexes in these three cases are equal to zero at 20.8 GHz according to Fig. 4(a). For Case #1 with an extremely thin DIL, the excessively large power leakage rate leads to a fast-decaying aperture field distribution. Despite achieving a radiation efficiency of 63.8%, the antenna's broadside gain is limited to 5.3 dBi, due to the restricted size of the effective aperture. In contrast, the over-thick DIL in Case #3 yields an excessively low power leakage rate, and thus the radiation efficiency is as low as 10.6%, resulting in a degraded realized gain of only 4.0 dBi. As shown in Fig. 5(b) and (e), the grating-loaded DIL design in Case #2 offers a relatively uniform leak-wave aperture, and it achieves a radiation efficiency of 68.5% and an enhanced broadside gain up to 17.1 dBi.

III. ANTENNA DESIGN, MEASUREMENT, AND DISCUSSION

By leveraging the low-attenuation NZI state of the grating-loaded DIL structure, this section proposes the design of an optically transparent leaky-wave antenna with high-gain broadside radiation

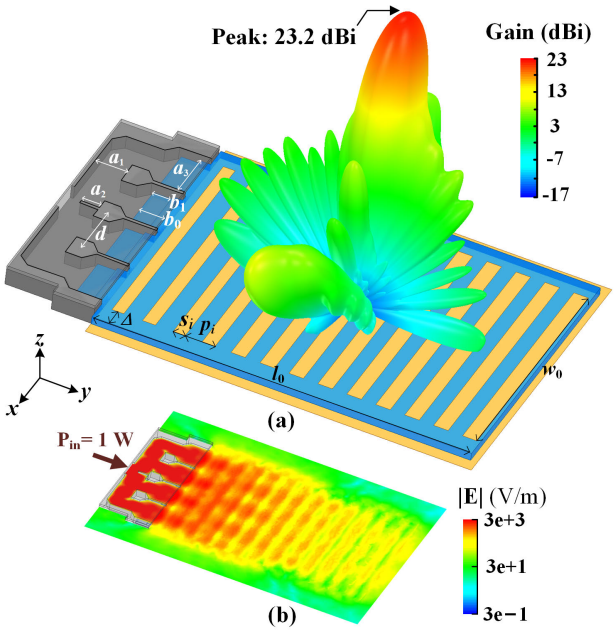

Fig. 6. (a) Prototyped OTA with simulated 3-D realized gain pattern. (b) Electric field magnitude distribution at 20.8 GHz.

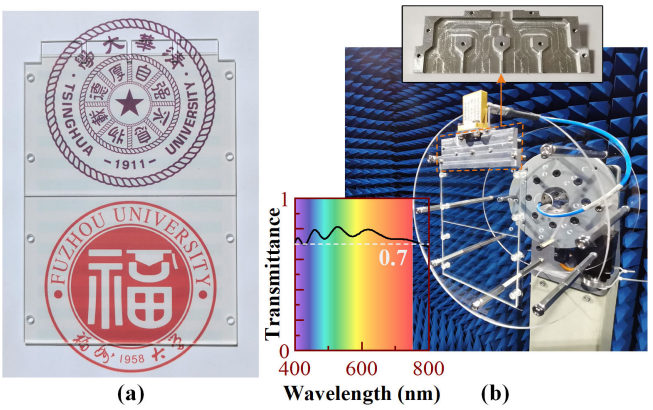

Fig. 7. Photograph of (a) optically transparent grating metamaterial and (b) fully assembled OTA.

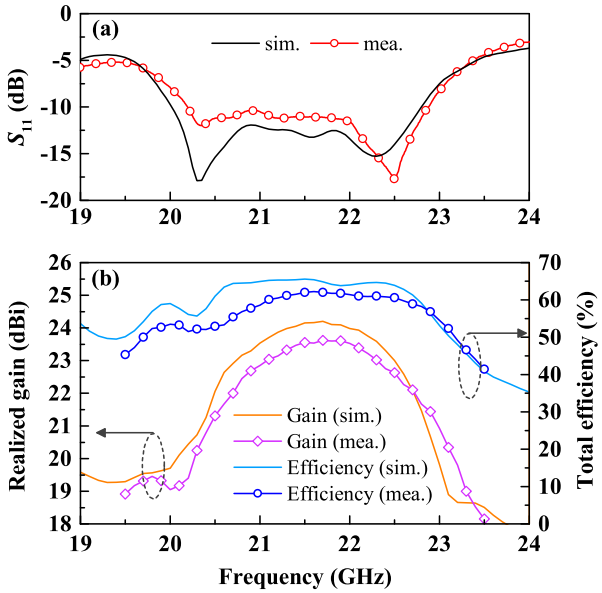

Fig. 8. (a) Reflection coefficients of the prototyped OTA. (b) Realized gain and total efficiency of the prototyped OTA.

performance. The proposed antenna structure is shown in Fig. 6(a), which consists of a transversely expanded TCF grating with a size of $l_0 \times w_0 = 8.18\lambda \times 5.27\lambda$ (at 20.8 GHz) and a grounded quartz glass substrate. The grating structure is excited by a compact 1:4 series-feed waveguide power divider. The step glass structures with upper and lower layer heights of $h_1 = 1$ mm and $h_2 = 1.5$ mm are introduced in the output waveguide branches for improving the mode transition from the power divider to the DIL structure. The heights of the grating-loaded DIL and the feeding waveguides are 2.5 and 4.3 mm, respectively. Local perturbations have been applied to the grating parameters, i.e., the strip width s_i and spacing p_i, for sidelobe suppression. The key structural parameters of the prototyped grating metamaterial antenna are listed in Table I.

The simulated 3-D realized gain pattern of the prototyped antenna at 20.8 GHz is also shown in Fig. 6(a), which validates that a directive beam with a peak gain of 23.2 dB is launched toward the near-broadside direction. The simulated electric field magnitude distribution over a plane slightly above the grating is shown in Fig. 6(b). The electric field is uniformly distributed over the first eight grating elements, which account for 60% of the total aperture area. This uniform aperture distribution is achieved through the precise control of the attenuation constant of the NZI grating metamaterial.

Fig. 7(a) displays the fabricated optically transparent grating-loaded DIL structure, where the grating pattern made of 5-Ω/sq ITO film is deposited on a 2.5-mm-thick quartz glass substrate. The ground of the prototyped DIL structure is a 2-Ω/sq ITO film. The thicknesses of the 5- and 2-Ω/sq ITO films are 270 and 680 nm, respectively. The skin depth of the ITO material with a bulk conductivity $\sigma_{\text{ITO}} = 7.4 \times 10^5$ S/m at 21 GHz is about 4.0 μm, which is significantly larger than the film thicknesses. Fig. 7(b) displays the assembled OTA with a four-way waveguide power divider. The waveguide power divider is made of aluminum and processed via the computer numerical control (CNC) metal machining technique. The whole assembled structure is fixed on a circular acrylic plastic panel, and it is connected to a standard WR-42 waveguide. The inset of Fig. 7 reports the averaged optical transmittance of the antenna aperture measured using a spectrophotometer. Over the visible spectrum of 400–760 nm, the mean value of the measured optical transmittance is 76%. Consequently, the proposed OTA based on ITO films and quartz glass is validated to offer a decent optical transmittance.

Fig. 8(a) shows the reflection coefficients (S_{11}) of the prototyped OTA. The measured −10-dB impedance bandwidth spans from 20.2 to 22.9 GHz, covering a fractional bandwidth of 12.5%. Fig. 8(b) reports the measured and simulated results of the OTA's realized gain. The measured (or simulated) realized gain reaches the peak value of 23.6 dBi (or 24.2 dBi) at 21.7 GHz. The 3-dB bandwidth for the measured realized gain covers 20.4–23.0 GHz. Fig. 8(b) also demonstrates the measured total efficiencies of the prototyped metamaterial OTA along with the simulated counterparts. The measured total efficiency attains a peak of 62% around the frequency of maximum gain radiation, where the measured radiation efficiency reaches 67%. The bandwidth for total efficiency exceeding 60% spans from 21.1 to 22.5 GHz. Fig. 9 demonstrates the OTA's directive radiation patterns at 20.3, 21.3, and 22.3 GHz. At these frequencies, the E-plane half-power beamwidths (HPBWs) of the OTA are 7.0°, 6.8°, and 6.5°, respectively, while the H-plane HPBWs are 10.2°, 10.0°, and 8.8°, respectively.

Table II shows comparison of the proposed OTA with state-of-the-art peripheral-fed directional OTAs in optical transmittance, realized gain, radiation efficiency, and aperture efficiency. In comparison to

TABLE II
COMPARISON OF THE PROPOSED OTA WITH STATE-OF-THE-ART PERIPHERAL-FED DIRECTIONAL OTA DESIGNS

Ref.	Antenna type	Operating band (GHz)[a]	Optical transmittance	Aperture area (λ_p^2)[b]	Peak realized gain (dBi)	Radiation efficiency[c]	Aperture efficiency[c]
[24] Ant. I[d]	1 × 8 Patch array	25.0–29.8	88%	1.96 × 4.85	6.7	24%	4.0%
[24] Ant. II[d]	1 × 8 Patch array	25.4–30.0	88%	1.96× 4.85	9.2	41%	7.0%
[49]	Ground-backed slot	1.89–2.24	71%	2.00 × 2.00	5.5	60%	7.1%
[48][d]	2 × 4 Patch array	56.4–62.0	68%	5.00 × 5.00	13.6	60%	7.3%
[2][d]	1 × 8 Monopole array	24.0–29.0	86%	1.95 × 3.90	9.7	61%	10.0%
[37]	Cavity-backed slot	24.0–28.4	71%	1.61 × 1.40	4.9	45%	11.0%
[7]	Traveling-wave antenna	7.50–10.0	80%	7.91 × 1.89	15.2	66%	17.6%
[23]	CRLH metamaterial	4.70–5.30	88%	2.41 × 0.29	2.7	63%	21.2%
This work[d]	Grating metamaterial	20.2–22.9	76%	8.54 × 6.37	23.6	67%	33.5%

[a]The reported frequency band for $|S_{11}| < -10$ dB. [b]λ_p is the wavelength at the frequency where the peak realized gain is realized.
[c]Measured at the frequency of the peak realized gain. [d]Power dividers are used for feeding.

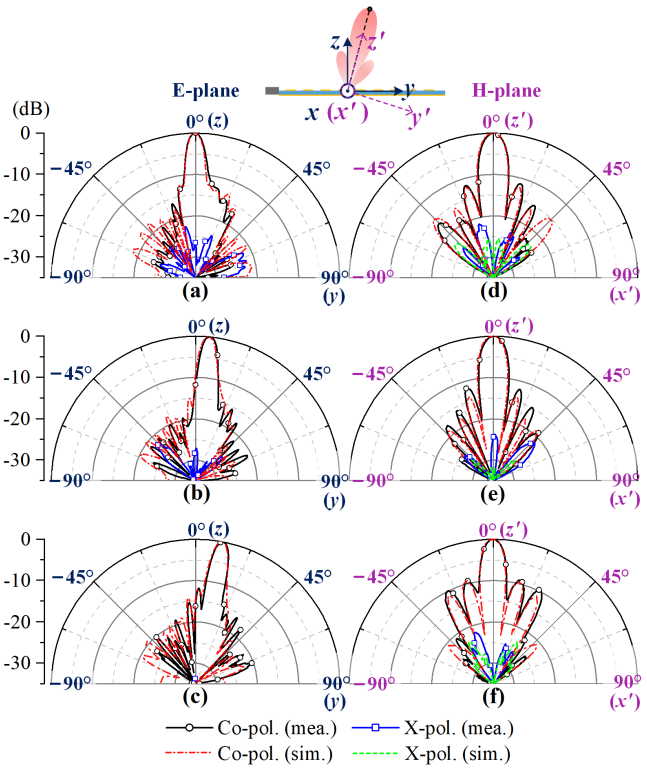

Fig. 9. Normalized E-plane radiation patterns of the OTA at (a) 20.3, (b) 21.3, and (c) 22.3 GHz. Normalized H-plane radiation patterns at (d) 20.3, (e) 21.3, and (f) 22.3 GHz.

the OTA designs based on resonant radiators such as the microstrip patch [24], [48], monopole [2], slot [37], [49], and the composite right/left-handed (CRLH) metamaterial [23], the proposed OTA design based on the leaky-wave metamaterial structure effectively avoids the severe ohmic loss issue arising at the resonance, thereby offering a competitive radiation efficiency. Moreover, in the proposed OTA array design, the antenna aperture is effectively extended in length by fine-controlling the complex propagation constant of the leaky-wave mode, while an adequate aperture width is ensured through the usage of a power divider. Overall, the proposed optically transparent metamaterial antenna based on the glass substrate grating structure delivers enhanced radiation performance in terms of realized gain and aperture efficiency.

IV. CONCLUSION

In conclusion, this work presents a feasible approach to launching high-gain broadside radiation on a lossy TCF. The proposed optical transparent radiator is based on an NZI grating metamaterial, which allows flexible manipulation of the phase progress and transverse confinement of the leaky-wave mode. By controlling the purely leakage-induced and total modal attenuations at the grating metamaterial's NZI state, our design realizes a competitive radiation efficiency and a uniform distribution of aperture fields on lossy TCFs. As a proof of the concept, an mmW OTA with an averaged optical transmittance of 76% is prototyped, which delivers a realized gain higher than 23 dBi and total efficiency exceeding 60% from 21.1 to 22.3 GHz. Compared with conventional resonant-type OTAs, the proposed OTA design based on the leaky-wave metamaterial realizes boosted gain and aperture efficiency. This improvement will enhance the mmW transceiving capability of transparent glass surfaces, facilitating a wide range of applications in ubiquitous wireless communication and sensing.

REFERENCES

[1] A. R. Chishti et al., "Optically transparent antennas: A review of the state-of-the-art, innovative solutions and future trends," *Appl. Sci.*, vol. 13, no. 1, p. 210, Dec. 2022.
[2] H. Qiu et al., "Compact, flexible, and transparent antennas based on embedded metallic mesh for wearable devices in 5G wireless network," *IEEE Trans. Antennas Propag.*, vol. 69, no. 4, pp. 1864–1873, Apr. 2021.
[3] W. Hong et al., "mmWave 5G NR cellular handset prototype featuring optically invisible beamforming antenna-on-display," *IEEE Commun. Mag.*, vol. 58, no. 8, pp. 54–60, Aug. 2020.
[4] Z. J. Silva, C. R. Valenta, and G. D. Durgin, "Optically transparent antennas: A survey of transparent microwave conductor performance and applications," *IEEE Antennas Propag. Mag.*, vol. 63, no. 1, pp. 27–39, Feb. 2021.
[5] O. R. Alobaidi, P. Chelvanathan, S. K. Tiong, B. Bais, M. A. Uzzaman, and N. Amin, "Transparent antenna for green communication feature: A systematic review on taxonomy analysis, open challenges, motivations, future directions and recommendations," *IEEE Access*, vol. 10, pp. 12286–12321, 2022.
[6] L. Cai, J. Zhou, H. Hu, X. Xu, Z. Hao Jiang, and W. Hong, "Indium-tin-oxide-based broadband optically transparent reflectarray antenna using a multilayer hybrid dielectric substrate and heterogeneous elements," *IEEE Trans. Antennas Propag.*, vol. 71, no. 11, pp. 9101–9106, Nov. 2023.
[7] Z. Zhou et al., "The low-attenuation endfire leaky-wave state on an optically transparent lossy film," *Engineering*, vol. 43, pp. 72–80, Dec. 2024.
[8] H.-R. Zu et al., "Optically and radiofrequency-transparent metadevices based on quasi-one-dimensional surface plasmon polariton structures," *Nature Electron.*, vol. 6, no. 7, pp. 525–533, Jul. 2023.

[9] J. Shu and Y. Zhang, "Tailoring meta-liquid crystal for larger tunability," *Electromagn. Sci.*, vol. 1, no. 4, pp. 1–10, Dec. 2023.

[10] Y. Feng, Q. Hu, K. Qu, W. Yang, Y. Zheng, and K. Chen, "Reconfigurable intelligent surfaces: Design, implementation, and practical demonstration," *Electromagn. Sci.*, vol. 1, no. 2, pp. 1–21, Jun. 2023.

[11] K.-M. Luk and B. Xiang, "Transmitarray and reflectarray antennas based on a magnetoelectric dipole antenna," *Electromagn. Sci.*, vol. 1, no. 1, pp. 1–14, Mar. 2023.

[12] Y. Zhang and Y. Li, "Wideband microstrip antenna in small, volume without using fundamental mode," *Electromagn. Sci.*, vol. 1, no. 2, Jun. 2023, Art. no. 0020073.

[13] B. Kim and J. Oh, "Single-glass-layer optically transparent transmitarray with high aperture efficiency and low profile at 5G millimeter-wave band," *IEEE Trans. Antennas Propag.*, vol. 71, no. 11, pp. 9036–9041, Nov. 2023.

[14] H. Chang, F.-P. Lai, and Y.-S. Chen, "Transparent transmitarray antenna with large aperture for significant gain enhancement in millimeter-wave 5G communication networks," *IEEE Antennas Wireless Propag. Lett.*, vol. 23, pp. 663–667, 2024.

[15] Y. Morimoto, S. Shiu, I. W. Huang, E. Fest, G. Ye, and J. Zhu, "Optically transparent antenna for smart glasses," *IEEE Open J. Antennas Propag.*, vol. 4, pp. 159–167, 2023.

[16] W. Zhu, X. Liu, Y. Fan, Z. Zhang, and X. Ma, "Transparent and flexible antenna with polarization reconfigurability using EGaIn for wearable applications," *IEEE Trans. Antennas Propag.*, vol. 72, no. 10, pp. 7493–7503, Oct. 2024.

[17] D. Potti et al., "A novel optically transparent UWB antenna for automotive MIMO communications," *IEEE Trans. Antennas Propag.*, vol. 69, no. 7, pp. 3821–3828, Jul. 2021.

[18] Y.-X. Sun, D. Wu, X. S. Fang, and J. Ren, "On-glass grid structure and its application in highly-transparent antenna for Internet of Vehicles," *IEEE Trans. Veh. Technol.*, vol. 72, no. 1, pp. 93–101, Jan. 2023.

[19] Z.-G. Liu, C. Zhang, R.-J. Yin, and W.-B. Lu, "Multifunctional low-profile Fabry–Perot resonator antenna integrated with solar cells," *IEEE Trans. Antennas Propag.*, vol. 70, no. 8, pp. 7175–7180, Aug. 2022.

[20] B. Xi, X. Liang, Q. Chen, K. Wang, J. Geng, and R. Jin, "Optical transparent antenna array integrated with solar cell," *IEEE Antennas Wireless Propag. Lett.*, vol. 19, pp. 457–461, 2020.

[21] T. D. Ha, L. Zhu, N. Alsaab, P.-Y. Chen, and J. L. Guo, "Optically transparent metasurface radome for RCS reduction and gain enhancement of multifunctional antennas," *IEEE Trans. Antennas Propag.*, vol. 71, no. 1, pp. 67–77, Jan. 2023.

[22] J. Oh, B. Kim, S. Yoon, K. Kim, E. J. Sung, and J. Oh, "High-gain millimeter-wave antenna-in-display using non-optical space for 5G smartphones," *IEEE Trans. Antennas Propag.*, vol. 71, no. 2, pp. 1458–1468, Feb. 2023.

[23] M. Kim et al., "Antenna-on-display concept on an extremely thin substrate for sub-6 GHz wireless applications," *IEEE Trans. Antennas Propag.*, vol. 70, no. 7, pp. 5929–5934, Jul. 2022.

[24] J. Park, S. Y. Lee, J. Kim, D. Park, W. Choi, and W. Hong, "An optically invisible antenna-on-display concept for millimeter-wave 5G cellular devices," *IEEE Trans. Antennas Propag.*, vol. 67, no. 5, pp. 2942–2952, May 2019.

[25] W. Hong, S. Lim, S. Ko, and Y. G. Kim, "Optically invisible antenna integrated within an OLED touch display panel for IoT applications," *IEEE Trans. Antennas Propag.*, vol. 65, no. 7, pp. 3750–3755, Jul. 2017.

[26] C. Ding, L. Liu, and K.-M. Luk, "An optically transparent dual-polarized stacked patch antenna with metal-mesh films," *IEEE Antennas Wireless Propag. Lett.*, vol. 18, no. 10, pp. 1981–1985, Oct. 2019.

[27] B. Chen, B. Wu, H.-R. Zu, J.-Q. Hou, and T. Su, "Experimental demonstration of high optically transparent reflectarrays using fine metal line structure," *IEEE Trans. Antennas Propag.*, vol. 70, no. 11, pp. 10504–10511, Nov. 2022.

[28] P. Duy Tung and C. W. Jung, "Optically transparent wideband dipole and patch external antennas using metal mesh for UHD TV applications," *IEEE Trans. Antennas Propag.*, vol. 68, no. 3, pp. 1907–1917, Mar. 2020.

[29] K. An, P. Sun, Y. Deng, and A. Chen, "A large-scale high-gain transparent grid array antenna for millimeter-wave communication," *IEEE Antennas Wireless Propag. Lett.*, vol. 23, pp. 1598–1602, 2024.

[30] P. Aghabeyki, P. de la Rosa, M. Caño-García, X. Quintana, R. Guirado, and S. Zhang, "Optically transparent beam-steering reflectarray antennas based on a liquid crystal for millimeter-wave applications," *IEEE Trans. Antennas Propag.*, vol. 72, no. 1, pp. 614–627, Jan. 2024.

[31] S. H. Kang and C. W. Jung, "Transparent patch antenna using metal mesh," *IEEE Trans. Antennas Propag.*, vol. 66, no. 4, pp. 2095–2100, Apr. 2018.

[32] F. Colombel, X. Castel, M. Himdi, G. Legeay, S. Vigneron, and E. M. Cruz, "Ultrathin metal layer, ITO film and ITO/Cu/ITO multilayer towards transparent antenna," *IET Sci., Meas. Technol.*, vol. 3, no. 3, pp. 229–234, May 2009.

[33] A. Desai and T. Upadhyaya, "Transparent dual band antenna with μ-negative material loading for smart devices," *Microw. Opt. Technol. Lett.*, vol. 60, no. 11, pp. 2805–2811, Oct. 2018.

[34] S. Hong, Y. Kim, and C. W. Jung, "Transparent UWB antenna with IZTO/Ag/IZTO multilayer electrode film," *Int. J. Antennas Propag.*, vol. 2016, pp. 1–8, Oct. 2016.

[35] C. Zhang et al., "Functional plastic films: Nano-engineered composite based flexible microwave antennas with near-unity relative visible transmittance," *Light, Adv. Manuf.*, vol. 5, no. 2, p. 1, 2024.

[36] S. Hong, Y. Kim, and C. W. Jung, "Transparent microstrip patch antennas with multilayer and metal-mesh films," *IEEE Antennas Wireless Propag. Lett.*, vol. 16, pp. 772–775, 2017.

[37] Y. Shi, W. J. Wang, and T. T. Hu, "A transparent SIW cavity-based millimeter-wave slot antenna for 5G communication," *IEEE Antennas Wireless Propag. Lett.*, vol. 21, no. 6, pp. 1105–1109, Jun. 2022.

[38] P. B. Samal, S. J. Chen, T. T. Tung, D. Losic, and C. Fumeaux, "Efficiency-driven design for planar antennas with lossy materials," *IEEE Open J. Antennas Propag.*, vol. 4, pp. 23–33, 2023.

[39] H. J. Song, T. Y. Hsu, D. F. Sievenpiper, H. P. Hsu, J. Schaffner, and E. Yasan, "A method for improving the efficiency of transparent film antennas," *IEEE Antennas Wireless Propag. Lett.*, vol. 7, pp. 753–756, 2008.

[40] M. R. Haraty, M. Naser-Moghadasi, A. A. Lotfi-Neyestanak, and A. Nikfarjam, "Improving the efficiency of transparent antenna using gold nanolayer deposition," *IEEE Antennas Wireless Propag. Lett.*, vol. 15, pp. 4–7, 2016.

[41] M. Lobet, I. Liberal, L. Vertchenko, A. V. Lavrinenko, N. Engheta, and E. Mazur, "Momentum considerations inside near-zero index materials," *Light, Sci. Appl.*, vol. 11, no. 1, pp. 1–8, Apr. 2022, Art. no. 110.

[42] L. Vertchenko, C. DeVault, R. Malureanu, E. Mazur, and A. Lavrinenko, "Near-zero index photonic crystals with directive bound states in the continuum," *Laser Photon. Rev.*, vol. 15, no. 7, May 2021, Art. no. 2000559.

[43] H. Li et al., "Geometry-independent antenna based on Epsilon-near-zero medium," *Nature Commun.*, vol. 13, no. 1, Jun. 2022, Art. no. 3568.

[44] Z. Zhou et al., "Dispersion coding of ENZ media via multiple photonic dopants," *Light, Sci. Appl.*, vol. 11, no. 1, pp. 1–11, Jul. 2022, Art. no. 207.

[45] D. M. Pozar, *Microwave Engineering*, 4th ed., Hoboken, NJ, USA: Wiley, 2011.

[46] A. Zandamela, A. Al-Bassam, and D. Heberling, "Circularly polarized periodic leaky-wave antenna based on dielectric image line for millimeter-wave radar applications," *IEEE Antennas Wireless Propag. Lett.*, vol. 20, pp. 938–942, 2021.

[47] J. Liu, D. R. Jackson, and Y. Long, "Substrate integrated waveguide (SIW) leaky-wave antenna with transverse slots," *IEEE Trans. Antennas Propag.*, vol. 60, no. 1, pp. 20–29, Jan. 2012.

[48] A. Martin, O. Lafond, M. Himdi, and X. Castel, "Improvement of 60 GHz transparent patch antenna array performance through specific double-sided micrometric mesh metal technology," *IEEE Access*, vol. 7, pp. 2256–2262, 2019.

[49] J. Hautcoeur, F. Colombel, M. Himdi, X. Castel, and E. M. Cruz, "Large and optically transparent multilayer for broadband H-shaped slot antenna," *IEEE Antennas Wireless Propag. Lett.*, vol. 12, pp. 933–936, 2013.